Available online at www.sciencedirect.com
ScienceDirect
Journal of Power Sources 180 (2008) 343–353
JOURNAL OF POWER SOURCES
www.elsevier.com/locate/jpowsour

Comparative finite element analysis of the stress–strain states in three different bonded solid oxide fuel cell seal designs

K.S. Weil *, B.J. Koeppel

Pacific Northwest National Laboratory, P.O. Box 999, Richland, WA 99352, United States

Received 7 December 2007; received in revised form 29 January 2008; accepted 31 January 2008
Available online 17 February 2008

Abstract

One of the critical issues in designing and fabricating a high performance planar solid oxide fuel cell (pSOFC) stack is the development of the appropriate materials and techniques for hermetically sealing the metal and ceramic components. A second critical issue is ensuring that the brittle ceramic cell constituents, i.e. the electrodes and electrolyte, exhibit high mechanical reliability by mitigating potential sources of thermal-mechanically induced stresses that can lead to fracture during operation and/or shutdown. A foil-based sealing approach is currently being developed that appears to offer good hermeticity and mechanical integrity, while minimizing the generation of high stresses in either of the joint's substrate materials. Based on the concept's viability, demonstrated in prior experimental work, numerical analyses were conducted to evaluate the behavior and benefits of the seal in a configuration prototypic of current pSOFC stack designs. This paper presents recent results from finite element (FE) simulations of a planar cell using the foil-based seal, along with companion analyses of the more conventionally employed glass-ceramic and brazed joints. The stresses and deformations of the components were evaluated at isothermal operating and shutdown temperatures. The results indicate that the foil seal is able to accommodate a significant degree of thermal mismatch strain between the metallic support structure and the ceramic cell via elastic deformations of the foil and plasticity in the foil-to-cell braze layer. Consequently the cell stresses in this type of seal are predicted to be much lower than those in the glass-ceramic and brazed designs, which is expected to lead to improved stack reliability. This ability to accommodate large thermal strain mismatches allows the design requirement of thermal expansion matching between ceramic and metal stack components to be relaxed and expands the list of candidate materials that can be considered for the metal frames and interconnects.

Keywords: Solid oxide fuel cell; Finite element analysis; Glass-ceramic seal; Brazed seal; Bonded compliant seal (BCS)

1. Introduction

A number of planar solid oxide fuel cell (pSOFC) stack designs currently under development employ a peripheral seal between the electrochemically active ceramic cell and an adjacent metal window frame component [1,2]. Along with a metal separator plate, which is typically brazed or welded to the frame prior to sealing the cell, this modular assembly forms the repeat unit in the overall stack [3,4]. Recent reviews by Fergus [5] and Weil [6] detail the various processes and materials often used in sealing pSOFCs. In general the window frame seal must be hermetic throughout the lifetime of the device, which is typically in the order of 10,000 h or more. During operation, the seals are nominally exposed to an oxidizing atmosphere on the cathode side and a wet reducing gas on the anode side at an average temperature of 750 °C. Because the electrical performance of the stack is directly proportional to the magnitude of the oxygen ion gradient that develops across the solid-state electrolyte, hermeticity is paramount. Gas leaks, either due to flaws that originate during stack manufacture or that form because of seal or component degradation during stack operation, lead to reductions in power output, electrical efficiency, and fuel utilization [7,8]. In addition they can cause local hot spots (or worse widespread deflagration) within the stack, both of which induce accelerated degradation in the device [7].

A new type of seal is being developed to offer stack designers greater flexibility in selecting materials for the window frame and separator plate components [9]. The seal, known as the bonded compliant seal (BCS), consists of a thin deformable metal foil bonded to the adjacent metal and ceramic components.

* Corresponding author. Tel.: +1 509 375 6796; fax: +1 509 375 2186.
E-mail address: Scott.Weil@pnl.gov (K.S. Weil).

0378-7753/$ – see front matter © 2008 Elsevier B.V. All rights reserved.
doi:10.1016/j.jpowsour.2008.01.093

It is expected to display the same level of hermeticity as glass and brazed seals, while offering greater accommodation of the stresses that arise in the ceramic cell due to thermal expansion mismatch with the adjacent metal components. Proof-of-concept testing showed that small-scale BCS joints retain their initial hermeticity and strength through numerous thermal cycles. Based on these results, a comprehensive design study was undertaken to determine the viability of this type of seal at a size and shape more prototypic of a full-scale stack. In the first phase of this study, reported here, the BCS was compared with a traditional glass-ceramic seal and the newly developed air braze seal [10] via finite element (FE) analysis to determine what advantages the BCS might offer in terms of stress/strain mitigation and/or reduced part deflection during a typical stack heating/cooling sequence.

2. Modeling parameters

Three-dimensional (3-D) FE analyses of the following three pSOFC seal designs were conducted using the ANSYS 10.0 software suite: (1) a typical barium aluminosilicate glass-ceramic seal, (2) a silver–copper oxide air brazed seal, and (3) the BCS. Depicted in Fig. 1(a)–(c) are cross-sectional representations of each seal type. Often oxidation resistant ferritic stainless steels are chosen for use in SOFC stack components because the thermal expansion of this class of material nearly matches that of the reduced ceramic cell. However nickel-based alloys, particularly alumina-scale formers, would offer a number of advantages if their thermal expansion could be accommodated via a compliant seal design. These advantages include greater oxidation and creep resistance, which will likely find greater importance in the coming years as stacks are tested to their anticipated operation lifetimes (>30,000 h), and reduction/elimination of chromia volatilization, a factor that leads to accelerated degradation of stack power. In this analysis, the ceramic cell is hypothetically sealed to a Haynes 214 window frame for all three seal designs. Haynes 214 was selected because it is representative of the type of nickel-based, alumina-scale-forming alloy that would be of particular interest in an SOFC stack design [11]. In addition it illustrates a worst-case scenario with respect to coefficient of thermal expansion (CTE) mismatch; i.e. its CTE is over 50% greater than that of an anode-supported cell (15.7 $\mu m\,m^{-1}\,K^{-1}$ vs. 10.6 $\mu m\,m^{-1}\,K^{-1}$) and therefore would present a significant materials joining challenge. Note that in the glass-ceramic and air brazed seal designs the cell is bonded directly to the metal frame, whereas in the BCS design the cell is air brazed to a stamped metal foil that in turn is brazed to a window frame using a conventional high-temperature braze such as AMS 4777, as shown in Fig. 1(c).

A finite element model that includes a window frame, seal, and anode structure was developed to evaluate the thermal–mechanical deformations and stresses of the joined assembly. For example in the BCS assembly, five components were modeled: (1) the cell, (2) the silver-brazed air braze filler metal layer, (3) the stamped Fecralloy foil, (4) the AMS 4777 filler metal layer, and (5) the Haynes 214 window frame. Eight-noded linear isoparametric brick elements with three translational degrees of freedom at each node were employed in constructing the FE meshes. A fine mesh was used in the regions of interest around the seal while a coarser mesh was judged sufficient to capture the overall structural response of the rest of the model. An enhanced strain formulation was used with the single layered elements to adequately capture the bending response. To investigate the location and magnitude of thermally generated mismatch stresses and out-of-plane deformations in each design, a uniform temperature load condition was applied to simulate operational and shutdown conditions. That is, the temperature value assigned to every node in the model was linearly ramped between the operation and shutdown temperatures to represent a thermal cycle, simulating the near isothermal condition that would result from testing in a furnace with a slow heating rate. In all three cases the component temperature was initially set to the joining temperature (1273 K, 1000 °C), which defined the

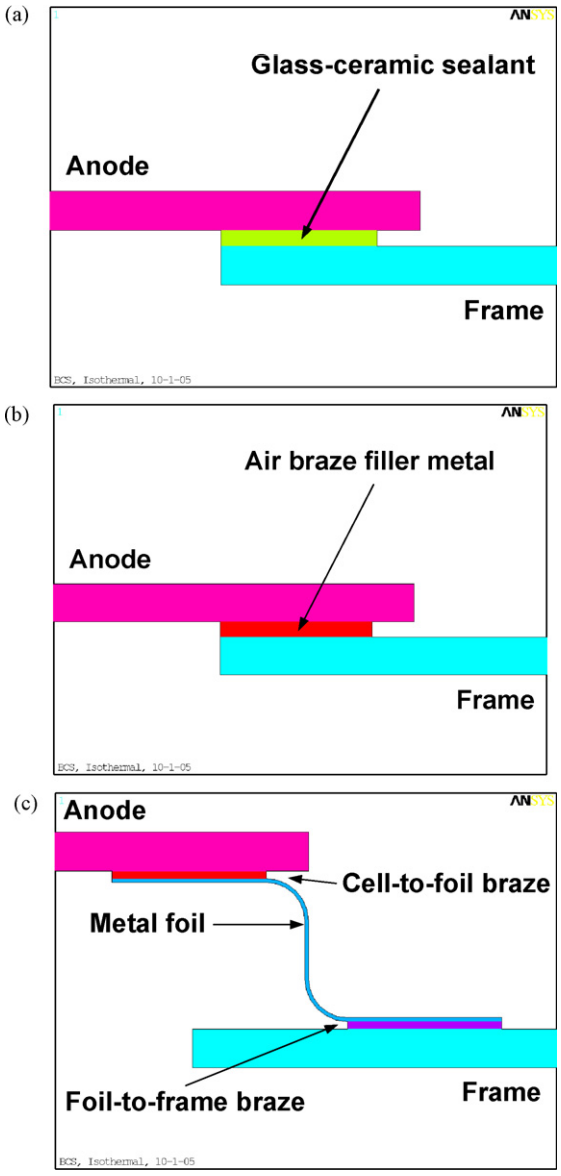

Fig. 1. Cross-sectional schematics of: (a) the glass-ceramic seal design, (b) the air brazed seal design, and (c) the BCS design.

Table 1
Component dimensions and materials database properties employed in modeling

Component	Thickness (μm)	Material
Glass-ceramic seal		
Cell	500	Ni–YSZ
Sealant	100	Barium aluminosilicate glass
Frame	500	Haynes 214
Brazed seal		
Cell	500	Ni–YSZ
Sealant	100	Silver
Frame	500	Haynes 214
Bonded compliant seal		
Cell	500	Ni–YSZ
Cell-to-foil braze	100	Silver
Metal foil	50	FeCrAlY
Foil-to-frame braze	100	BNi-2 braze
Frame	500	Haynes 214

stress-free state, cooled to an assumed operating temperature of 1073 K (800 °C), and finally cooled to room temperature (298 K, 20 °C). The boundary conditions used in the analysis were: (1) the application of symmetry conditions for a one-quarter model to minimize computational time and data storage space (consequently, all of the computational maps reported here are shown as quarter-symmetry representations) and (2) the out-of-plane displacements for the bottom of the window frame were constrained to zero, permitting only 2-D in-plane deformations. However in each case, out-of-plane component deflections were allowed throughout the rest of the model.

While the cells employed in a fully operational stack are composed of three layers, a Ni–YSZ anode (typically 450–570 μm thick), a dense electrolyte (5–8 μm thick), and a perovskite cathode (e.g. lanthanum strontium manganate; typically 15–20 μm thick), a simplifying approximation was employed in which the mechanical properties of the cell were assumed to be those of the dominant layer. That is, the ceramic cell was modeled as a porous anode monolith measuring 500 μm thick × 120 mm square with 10 mm radii corners; dimensions that approximate the size of cells used in several stack designs currently under commercial development [12,13]. Listed in Table 1 are the thicknesses and compositions of the seal components that were employed in the analysis of each seal design. In the case of the glass-ceramic and air brazed seals, the seal thicknesses represent averages measured in actual stacks fabricated at Pacific Northwest National Laboratory. The structural contribution of the current collector and interconnect geometry will also influence the resulting deformation and stresses of the SOFC cell, but this model assumed a highly porous interconnect material is used, which offers little resistance to out-of-plane deformation.

The ANSYS general finite element analysis program is convenient because it allows the input of user defined constitutive models as well as control routines to obtain a convergent solution. With the exception of the cell, the mechanical properties of the remaining metallic components were treated using a bilinear elastic–plastic constitutive model with kinematic hardening. That is, the elastic modulus was used to describe stress–strain behavior up to the point of yielding, beyond which an average value of hardening modulus provided the increase in flow stress in the plastic regime. In this way, a set of temperature dependent stress–strain equations could be developed for each constituent material. The data used in these equations were obtained from the alloy manufacturers and/or reference handbooks [14–16]. The corresponding stress–strain curves are shown in Fig. 2(a)–(d). In the case of the anode material, elastic property data generated from ultrasonic pulse-echo testing of the reduced Ni–YSZ cermet at various temperatures was employed [17]. Modulus of rupture (MOR) data obtained at PNNL on a standard barium aluminosilicate glass in the as-joined condition [18] was used in modeling the mechanical behavior of the glass-ceramic sealant. CTE curves for each material were also obtained from either reported manufacturer's data or through in-house testing [14–16]. In the present comparative analysis, material creep was not considered.

3. Results and discussion

3.1. Comparative stress and strain analyses

Shown in Fig. 3 are the maximum principal stresses predicted in the cell when each sealing design is cooled from a stress-free state at 1273 K to an operating temperature of 1073 K (Fig. 3(a)–(c)) and then further to room temperature (Fig. 3(d)–(f)). In the case of the glass-ceramic sealant (Fig. 3(a) and (d)), the highest stresses initially develop in narrow regions of the cell (noted in red in both figures) just in-board of the cell-to-sealant joint along the *x*- and *y*-medians of the full-size cell. These stresses are due to in-plane tension developed perpendicular to the seal length. The finding is similar but higher in magnitude to that reported by Lin et al. for rectangular-shaped glass-sealed pSOFC stacks that employ stainless steel window frame components [19]. Also note that these areas of stress concentration do not appear to shift significantly with temperature. The maximum stresses calculated at 1073 and 298 K (summarized in Table 2) are well beyond the average fracture strength of many anode-supported cells, which are typically in the order of 200–300 MPa at room temperature and 150–250 MPa at 1073 K [20–22]. That is, conditions leading to cell fracture are predicted to occur when a Haynes 214 frame material is glass-sealed to a ceramic SOFC cell.

The predicted cell stresses result directly from: (1) the thermal expansion mismatch between the cell and window frame materials and (2) the lack of stress relief in this design (outside of a small amount of yielding in the Haynes 214 frame) due to the stiff elastic behavior of both the ceramic cell and sealant materials. In addition, as given in Table 2 the maximum stresses in the glass sealant at 1073 and 298 K are predicted to be 104 and 586 MPa, respectively. The latter is over seven times greater the average MOR for the crystalline glass, measured to be 83.1 MPa at room temperature [18], indicating a second potential mode of failure in this particular seal design. As noted in Fig. 4(a), there is a significant amount of stress across the entire sealing footprint at both 1073 and 298 K, with particularly high levels concentrated at the inner median edges. These stresses arise because

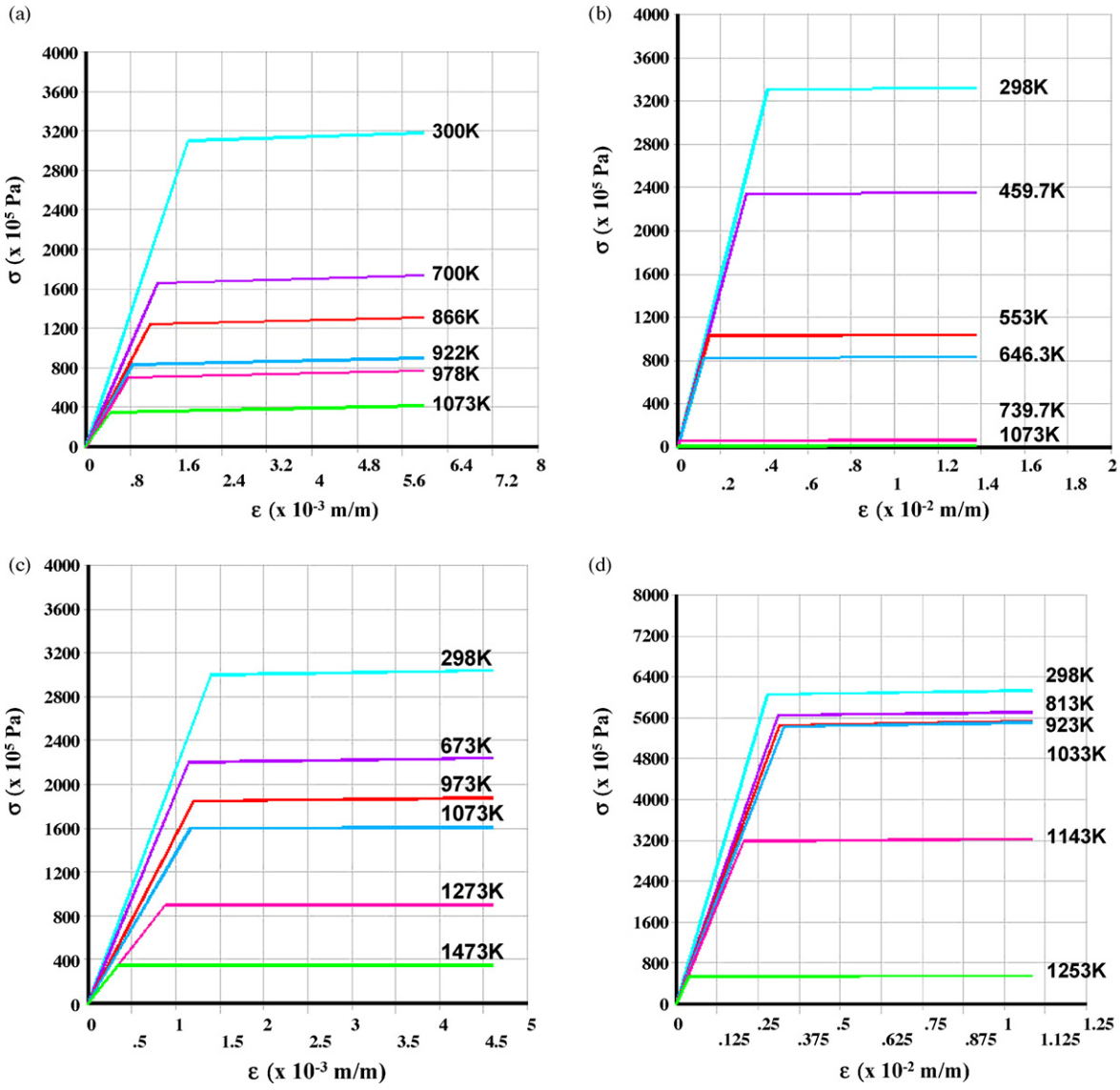

Fig. 2. Examples of the bilinear stress–strain curves employed in FE analysis: (a) FeCrAlY (Fecralloy foil), (b) Ag–CuO air braze (between the foil and YSZ electrolyte layer on the cell), (c) BNi-2 braze (between the separator and foil), and (d) Haynes 214 (used in the separator plate).

of the inability of the sealant material to exhibit any significant compliance due to plasticity or creep. The glass-ceramic material is capable of exhibiting only very limited strain prior to fracture at both the 1073 and 298 K thermal conditions. From tensile test data collected on a typical barium aluminosilicate glass-ceramic in the as-formed (i.e. partially crystallized) condition, the maximum strains at 1073 and 298 K are 0.80 and 0.13%, respectively and both values decrease somewhat with exposure time at 1073 K [18].

Alternatively, only modest stresses arise in the brazed cell under normal operating conditions, as seen in Fig. 3(b). When cooled from the sealing temperature to an operating temperature of 1073 K, the cell stresses in the brazed seal design are more than an order of magnitude lower than those generated in the

Table 2
Summary of maximum component stresses, strains, and deflections in each seal design

Seal design	Maximum stress in cell[a] (MPa)	Maximum deflection in cell (mm)	Maximum stresses in seal components (MPa)
Glass-ceramic seal	354/1160[b]	2.65/3.61[b]	104/586[b] (glass-ceramic)
Silver-based air braze seal	19/459	0.02/1.36	22/362 (filler metal)
BCS	24/90	0.82/2.41	3/238 (silver filler metal) 92/453 (FeCrAlY foil) 160/230 (BNi-2)

[a] The fracture stress for the cells range from 150 to 250 MPa at 1073 K and 200 to 300 MPa at 298 K [20–22].
[b] The first value reported is at 1073 K, the second is at 298 K.

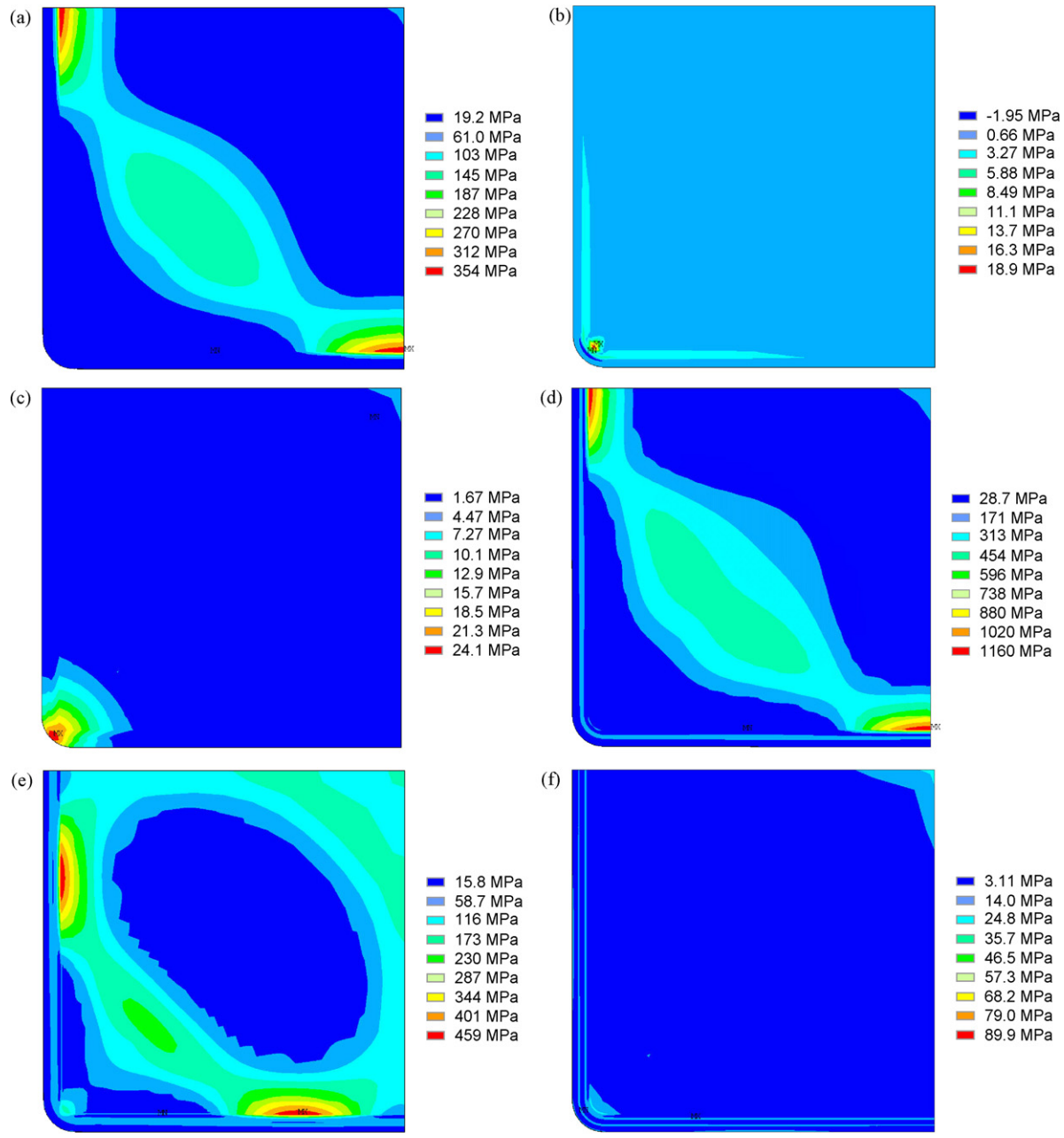

Fig. 3. Cell stress distributions predicted upon cooling from a stress-free state at 1273 K to: (a) 1073 K for the glass-ceramic seal design, (b) 1073 K for the air brazed seal design, (c) 1073 K for the BCS design, (d) 298 K for the glass-ceramic seal design, (e) 298 K for the air brazed seal design, and (f) 298 K for the BCS design.

glass-seal design and well within the range that can generally be tolerated by most anode-supported cells. Based strictly on a stress criterion, this seal design would be expected to perform well at this temperature because the silver-based sealing material plastically yields and thereby mitigates the build up of deleterious stresses in the adjacent cell and frame components. Similarly the von Mises stresses predicted within the silver-based seal are also quite low due to in situ annealing, as summarized in Table 2 and shown in Fig. 4(b). From Fig. 5(a) it can be seen that this is because the seal undergoes substantial plastic strains, upwards of 0.42×10^{-2} m m^{-1} in the corners of the seal. That is, the thermally induced mismatch strains are effectively transferred to the ductile metal seal.

However as shown in Fig. 3(e), a non-uniform stress distribution is predicted to arise in the cell upon cooling to room temperature, as the thermomechanical response of the silver changes from nearly purely plastic to one that is strongly elastic over this temperature range. The maximum cell stresses are concentrated primarily in-board of the brazed joint at regions approximately 2/3 the distance between the corner and the median axes of the cell. Although these stresses are nearly three times lower than those generated in the glass-seal design, they are still predicted to be higher than the average fracture strength of the cell [17,20,21]. This level of stress is again due to the mismatch in thermal expansion between the cell and window frame materials in the absence of sufficient mechanical compliance from the interme-

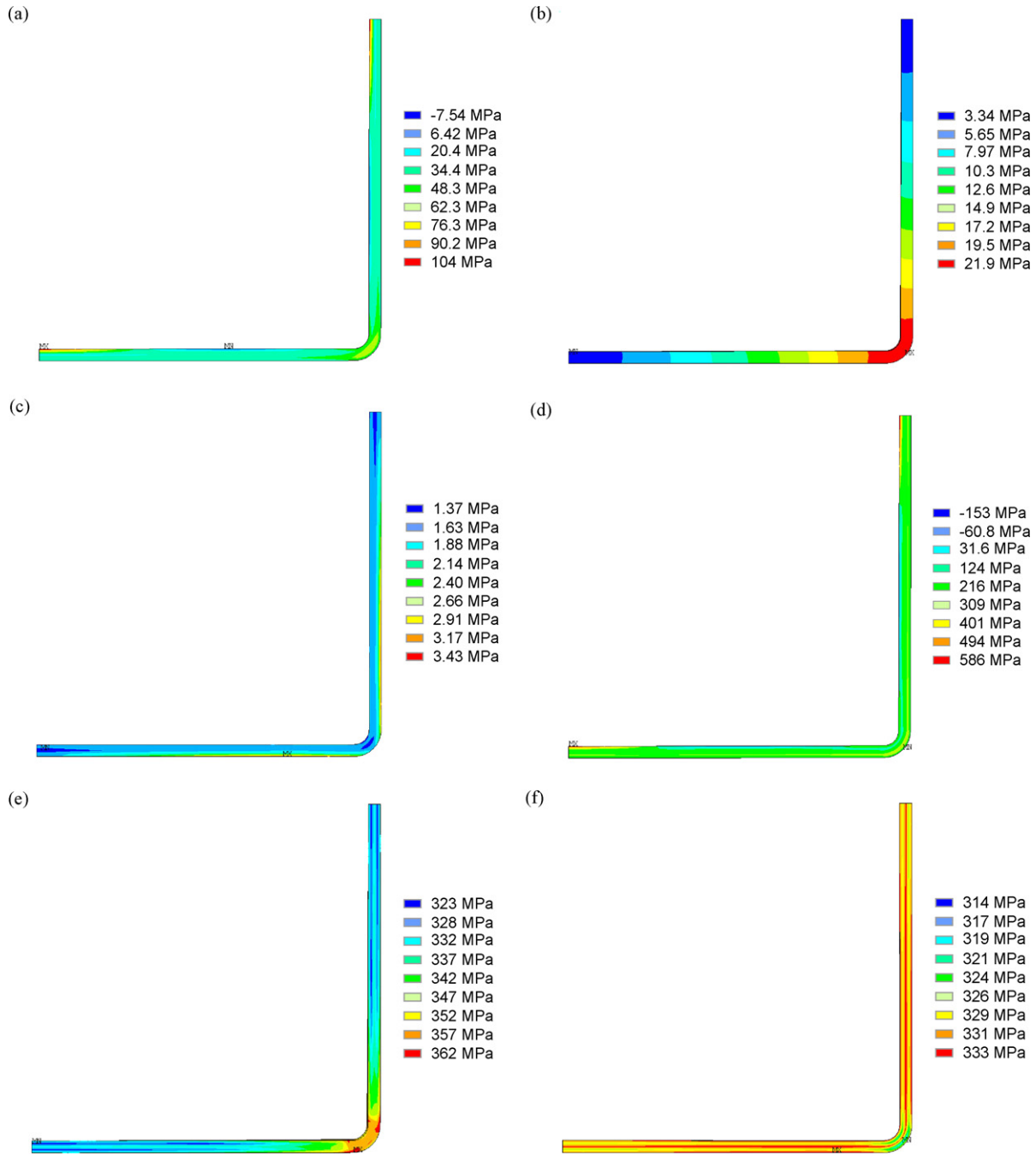

Fig. 4. Sealant stress distributions predicted upon cooling from a stress-free state at 1273 K to: (a) 1073 K for the glass-ceramic seal design, (b) 1073 K for the air brazed seal design, (c) 1073 K for the BCS design, (d) 298 K for the glass-ceramic seal design, (e) 298 K for the air brazed seal design, and (f) 298 K for the BCS design. Note the BCS component represented in (c) and (f) is the silver-based cell-to-foil filler metal.

diary silver-based seal. Both the dimensional mismatch between the components and the yield strength of the seal increase upon cooling. Thus while the silver-based sealing material does undergo some plastic deformation, it is not enough to accommodate the differential shrinkage that occurs between the cell and window frame. It should be noted that plastic deformation of the sealant would lead to a reduction in the maximum stresses of the various sealing components during a second thermal cycle [22]. However numerous such thermal cycles may lead to creep of the sealing material and possibly loss of hermeticity [23].

By comparison in the BCS seal design, stress accommodation occurs at both the operating temperature and room temperature. As shown in Fig. 3(c), at 1073 K the stresses in the cell are slightly higher than and similarly concentrated in the brazed seal design; although they are still well below the average fracture strength of the cell at this temperature. Stress concentration is predicted to begin occurring near the corners of the cell in the BCS design. At room temperature, the highest levels of cell stress are anticipated to arise in a band located directly adjacent to the foil-to-cell joint and are spread fairly uniformly in this narrow

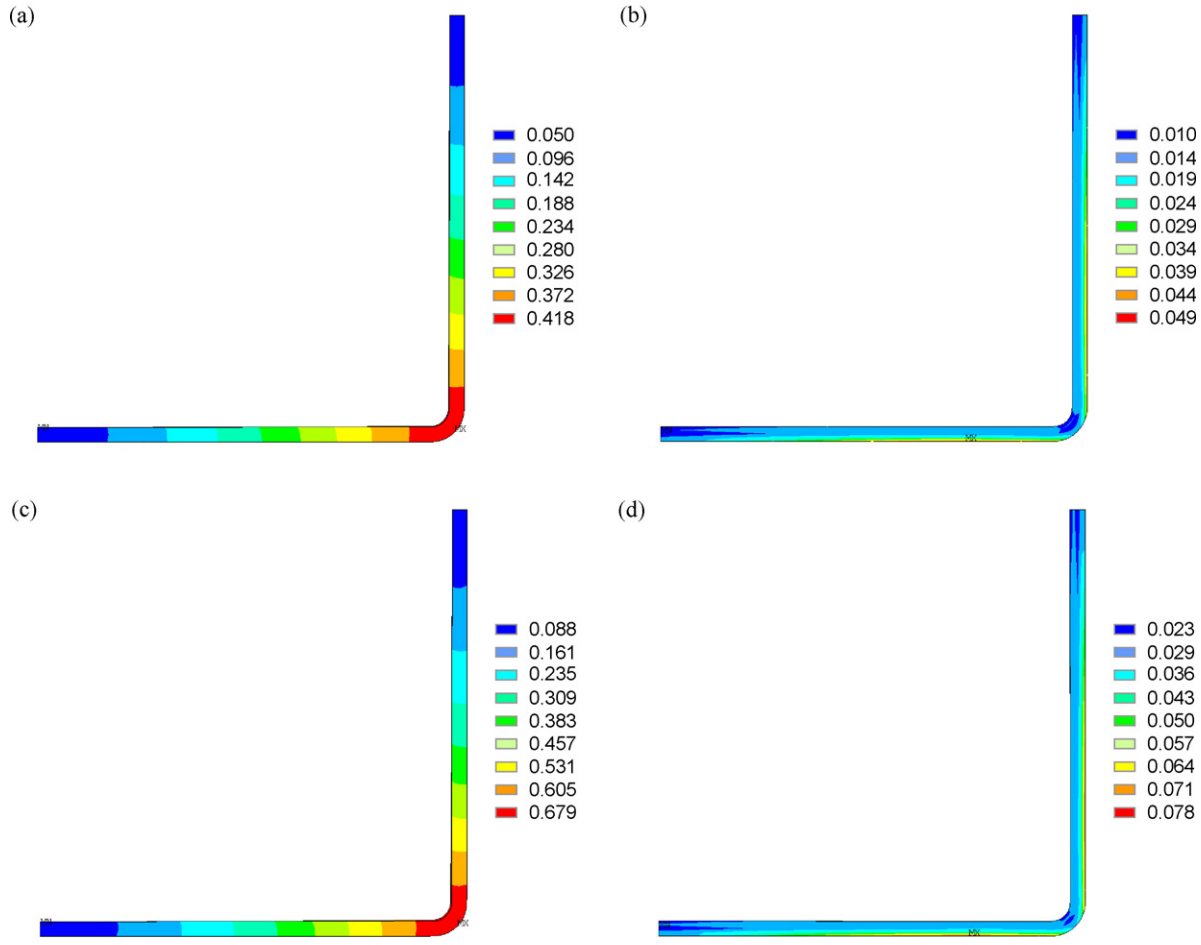

Fig. 5. Sealant strain distributions (in 10^{-2} m m^{-1}) predicted upon cooling from a stress-free state at 1273 K to: (a) 1073 K for the air brazed seal design, (b) 1073 K for the BCS design, (c) 298 K for the air brazed seal design, and (d) 298 K for the BCS design. Note the BCS component represented in (b) and (d) is the silver-based cell-to-foil filler metal. Note that the elastic limit for silver at room temperature is $\sim 0.4 \times 10^{-2}$ m m^{-1} (see Fig. 2(b)).

region. Outside of this band, the stresses are relatively uniform particularly in comparison with the other two seal designs.

As shown in Fig. 4(e) and (f) and in Figs. 5 and 6, an analysis of the von Mises stresses and equivalent total strains calculated in the BCS components at operating and room temperature indicates that deformation in both the metal foil and the silver-based braze filler metal between the foil and cell largely accommodates the expansion mismatch between the cell and frame components. The silver-based cell-to-foil filler metal undergoes nearly uniform strain and the sealing foil plastically stretches within the vertical section between the upper and lower sealing surfaces (see Fig. 1) and also collapses elastically, as shown in Fig. 7. In particular note in comparing Fig. 5(b) and (d) with Fig. 5(a) and (c) that the strains in the silver-based braze material are an order of magnitude smaller in the BCS design than in the brazed seal design. As will be discussed, one consequence of this mode of deformation is bowing in the cell. However, a second result is that the maximum stresses for the cell in the BCS design reported in Table 2 are substantially lower at room temperature than those predicted in the glass-ceramic and brazed seal designs. The largest stresses and strains in the overall BCS structure are localized within the deformable foil and the air braze. That is, the seal generally appears to function as designed by displacing excessive thermally induced strains away from cell and window frame and concentrating them as elastic and plastic strain within the thin sealing foil and the adjacent soft silver filler metal. There is a concurrent paper that examines possible design variations in the BCS and reports on the effects of metal foil thickness and shapes on the stress/strain distributions the various sealing components [22].

3.2. Comparative cell deflection analyses

Shown in Figs. 8 and 9 are planar and cross-sectional views of the out-of-plane deformation, or bowing, predicted in the cell for each seal design. The results given in Fig. 8(a)–(c) and (d)–(f) display the amount of cell deformation (red: out of the paper and dark blue: into the paper) upon cooling to 1073 and 298 K, respectively. Fig. 9(a)–(c) provide cross-sectional views of the various deformed cells along diagonal and medial sections, as predicted after cooling to 298 K. The maximum amount of out-of-plane deformation in each case is reported in Table 2. Two observations are immediately noted: (1) some degree of out-of-plane cell deformation is predicted in all three seal designs and

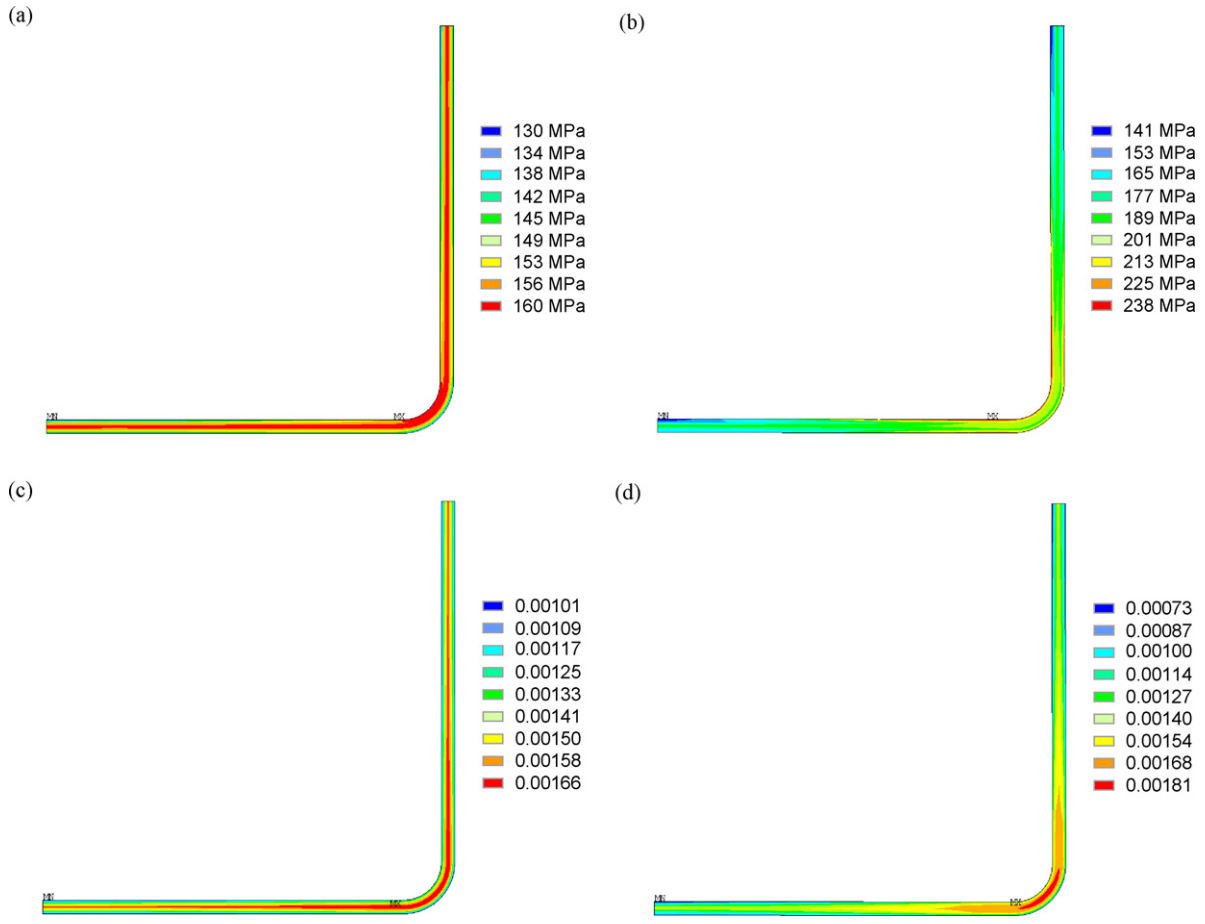

Fig. 6. Stress distributions predicted in the BCS metal foil upon cooling from a stress-free state at 1273 K to: (a) 1073 K and (b) 298 K. Strain distributions (in 10^{-2} m m^{-1}) predicted in the BCS metal foil upon cooling from a stress-free state at 1273 K to: (c) 1073 K and (d) 298 K.

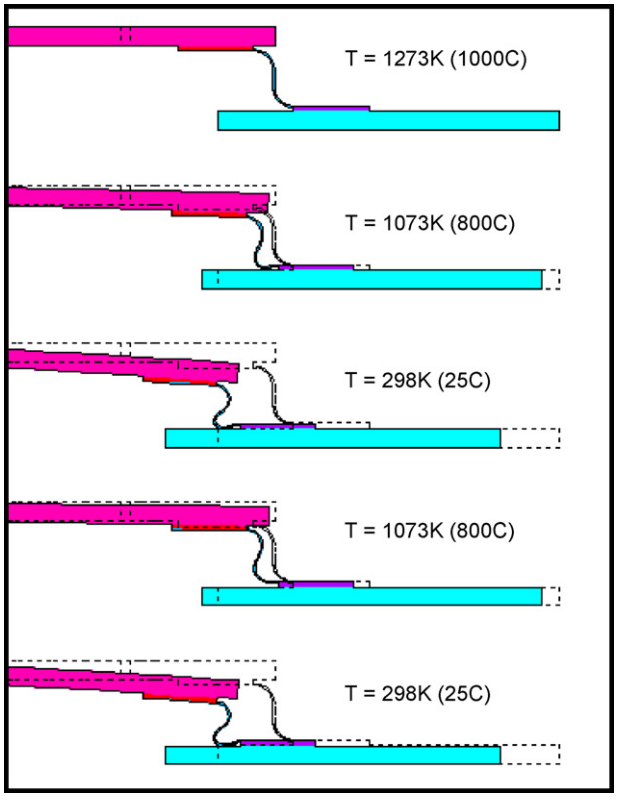

(2) the BCS design leads to the simplest mode of cell flexure at both high and low temperature, whereas the other two seals involve more complex modes of deflection in the ceramic cell. For example, of the three seal designs the glass-ceramic seal is predicted to display the largest amount of cell deflection over the entire range of 298–1073 K. This occurs due to the lateral compression of the anode from the greater thermal shrinkage of the metallic frame upon cooling. As this seal cannot accommodate any of the mismatch strains, the lateral compression causes anode deformations characteristic of plate buckling where the deformed shape is a function of the edge boundary constraint and the out-of-plane support. The out-of-plane support representing the mechanical stiffness of the interconnect geometry is the same for all of the models, but the effective translational and rotational stiffnesses of the anode edges will be different for each seal assembly. This can be observed in Figs. 8(a) and (d) and 9(b) where the cell exhibits different modes of deformation for each seal assembly. This suggests that designing the stiffness of the interconnect geometry in conjunction with the seal will

Fig. 7. A series of cross-sectional images based from FE analysis depicting how the BCS components change in size and shape at the corner of the seal as a function of cooling from the stress-free state at 1273 K to room temperature and upon re-heating to 1073 K and cooling back to room temperature. The original size/shape of the components at the stress-free state are denoted by the dotted lines.

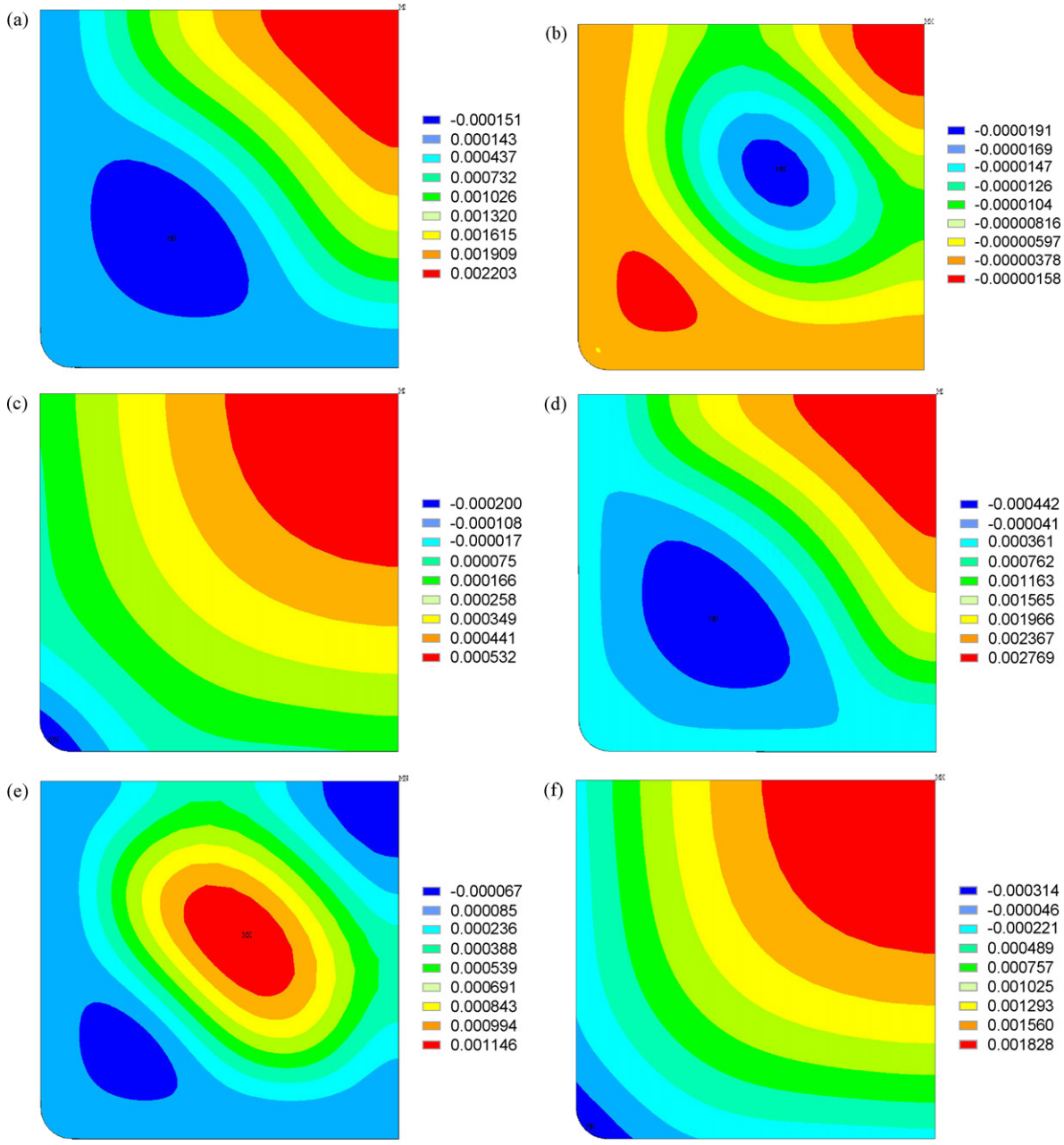

Fig. 8. Quarter-symmetry planar representations of cell deflection (in m) upon cooling from a stress-free state at 1273 K to: (a) 1073 K for the glass-ceramic seal design, (b) 1073 K for the air brazed seal design, (c) 1073 K for the BCS design, (d) 298 K for the glass-ceramic seal design, (e) 298 K for the air brazed seal design, and (f) 298 K for the BCS design.

be necessary to achieve the desired balance between control of the anode deflection and induced stresses.

While the brazed seal design is predicted to display the lowest amount of cell deflection, the mode is complex with multiple nodes predicted along each diagonal. In addition, the pattern of cell deflection in this seal design reverses as it is cooled from 1073 to 298 K. At 1073 K, the cell bows slightly outward at the center and the corners and bows inward at points roughly halfway in between. However the deformation mode predicted at operating temperature reverses completely at 298 K, as the cell deflects inward at the center and corners and bows outward at the quarter points along each diagonal. In the case of the BCS design, out-of-plane deflection is manifested as simple bowing with a maximum predicted at the center of the cell; 0.82 mm of bowing at 1073 K and 2.41 mm of bowing at room temperature over the entire 170 mm diagonal span. While the amount of deflection is somewhat higher than that predicted in the brazed seal design, the mode is far simpler and does not undergo a reversal during cooling or re-heating.

Although cell bowing is not desired, some amount of simple part deflection generally can be tolerated by the components or accommodated in the stack design. The amount of allowable bowing is dependent on specific features of the stack which were not included in this simplified model, e.g. allowable tol-

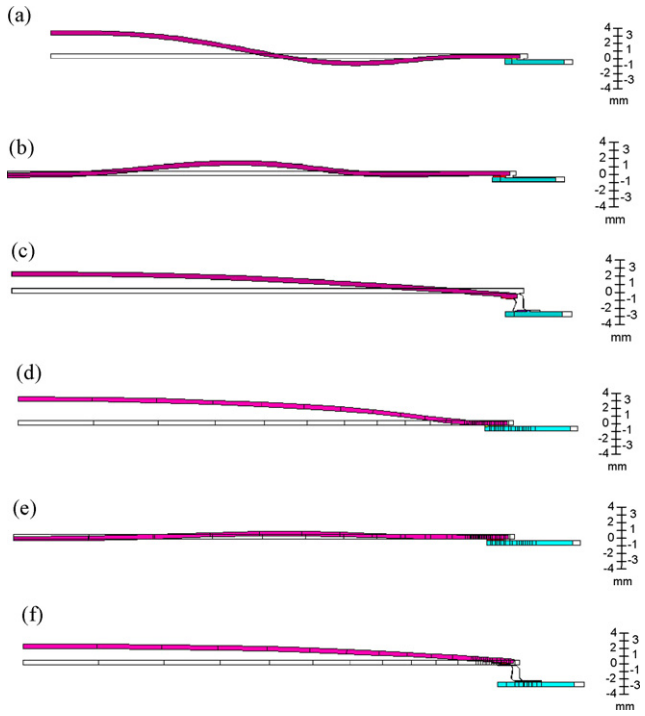

Fig. 9. Cross-sectional representations of cell deflection (in mm) upon cooling from a stress-free state at 1273 to 298 K for: (a) the glass-ceramic seal design along the diagonal, (b) the air brazed seal design along the diagonal, (c) the BCS design along the diagonal, (d) the glass-ceramic seal design along the mid-plane, (e) the air brazed seal design along the mid-plane, and (f) the BCS design along the mid-plane. Note that the original size/shape of the components at the stress-free state are denoted by the solid black lines.

erances in the fuel flow cavity, the type of interconnect being used, etc. Additionally, the modulus of the cell will strongly impact the amount of bowing/flexing to which the cell can be subjected and this can be tailored to some degree by changing the Ni/YSZ ratio in the anode, by modifying the thicknesses of the constituent layers, and/or by adding inert fillers such as Al_2O_3 [24,25]. However, it is anticipated that multi-modal forms of cell warpage of the type seen in Fig. 8(a)–(d) and in Fig. 9(a) and (b) are likely to cause gas flow maldistribution, problems with electrical contact, and deleterious interfacial strains within the multilayer ceramic part.

While the present analysis indicates that the BCS design clearly offers potential advantages over the glass-ceramic and brazed seal designs, there are limitations to these models including ignoring potential creep effects and assuming a completely uniform temperature distribution. It is expected that creep will tend to reduce stresses in the thinnest and least refractory components: the sealing foil, the cell-to-foil filler metal, and to some extent the nickel-based anode. In this regard the above model likely overestimates the maximum stresses in these components. Accurately predicting the temperature distribution within the stack and across the various stack components can be quite complex, even under steady-state conditions. A proper analysis should include heat generation due to the electrochemical reaction, enthalpy changes due to steam reformation, and the heat removal effects of water generation across the anode among other considerations. Over the past few years, pSOFC models of increasing sophistication have been reported [26–28] and a next generation BCS design analysis that utilizes thermal field prediction due to electrochemical operation can begin to account for the effects of non-uniform temperature distribution on thermal mismatch stresses/strains.

4. Conclusions

As a potential means of sealing SOFC components that exhibit a high degree of CTE mismatch, the BCS design offers obvious advantages over glass-ceramic and braze sealing, including significant reductions cell and sealant stresses and a simplification in the mode of planar cell deflection. This is because much of the mismatch strain between the metallic support/manifold structure and the ceramic cell is accommodated by elastic and plastic deformation within the sealing foil and adjacent silver-based braze filler metal. In-plane along the cell edge, the sealing foil undergoes elastoplastic deformation without buckling. In-plane perpendicular to the cell edge and out-of-plane, the foil accommodates much of the thermal expansion mismatch between the cell and separator via elastic–plastic deformation, although geometric non-uniformities (i.e. the corners) account for a significant amount of bowing predicted in the cell. However, the accommodation of these thermal strains results in significant stress reduction in the ceramic anode structure. Since crack growth and fracture of the brittle ceramic cell is the most significant mechanical design challenge for the SOFC, reduced stresses will lead to much improved reliability. Therefore, the BCS seal is an effective design modification that can be used either to increase the structural reliability of existing SOFC designs or permit usage of additional candidate interconnect materials by loosening the restrictions on CTE-matching.

Acknowledgements

This work was supported by the U.S. Department of Energy as part of the SECA Program. The Pacific Northwest National Laboratory is operated by Battelle Memorial Institute for the United States Department of Energy (U.S. DOE) under Contract DE-AC06-76RLO 1830.

References

[1] N. Christiansen, S. Kristensen, H. Holm-Larsen, P.H. Larsen, M. Mogensen, P.V. Hendriksen, S. Linderoth, Solid Oxide Fuel Cells IX, 2005, p. 168.
[2] L. Blum, H.-P. Buchkremer, L.G.J. de Haart, H. Nabielek, J.W. Quadakkers, U. Reisgen, R. Steinberger-Wilckens, R.W. Steinbrech, F. Tietz, I. Vinke, Ceram. Eng. Sci. Proc. 25 (3) (2004) 219.
[3] S. Mukerjee, K. Haltiner, S. Shaffer, K. Meinhardt, L. Chick, V. Sprenkle, S. Weil, J.Y. Kim, Solid Oxide Fuel Cells IX, 2005, p. 48.
[4] M. Stelter, A. Reinert, B.E. Mai, M. Kuznecov, J. Power Sources 154 (2006) 448.
[5] J. Fergus, J. Power Sources 147 (2005) 46.
[6] K.S. Weil, JOM 58 (2006) 37.
[7] T. Iwata, Y. Enami, J. Electrochem. Soc. 145 (1998) 931.
[8] J. Hartvigsen, J. Milliken, S. Elangovan, A. Khandkar, Ceramic Transactions, vol. 65, American Ceramic Society, Westerville, OH, 1996, p. 279.

[9] K.S. Weil, J.S. Hardy, B.J. Koeppel, J. Mater. Eng. Perform. 15 (2006) 427.
[10] K.S. Weil, J.Y. Kim, J.S. Hardy, Electrochem. Solid State Lett. 8 (2005) A133.
[11] Z. Yang, K.S. Weil, D.M. Paxton, J.W. Stevenson, J. Electrochem. Soc. 150 (A1188) (2003).
[12] S. Mukerjee, S. Shaffer, J. Zizelman, L. Chick, S. Baskaran, C. Coyle, Y.-S. Chou, J. Deibler, G. Maupin, K. Meinhardt, D. Paxton, T. Peters, V. Sprenkle, S. Weil, Eighth International Symposium Solid Oxide Fuel Cells, v. 2003, The Electrochemical Society, 2003.
[13] N.Q. Minh, P. Kelly, K. Montgomery, Second European Solid Oxide Fuel Cell Forum Proceedings, vol. 2, pt. 2, 1996, p. 659.
[14] Haynes International, Inc., Report # H3008C, available from www.haynesintl.com/ HTAlloys.htm#214, 1996.
[15] S. Chang, Engineered Materials Solutions, www.emsclad.com, 2005, personal communication.
[16] Metals Handbook, vols. 2 and 3, ninth ed., American Society for Metals, 1980.
[17] B.J. Koeppel, J.S. Vetrano, B.N. Nguyen, X. Sun, M.A. Khaleel, Advances in Solid Oxide Fuel Cells. II: A Collection of Papers Presented at the 30th International Conference on Advanced Ceramics and Composites, 2006, p. 325.
[18] K. D. Meinhardt, D-S. Kim, Y-S. Chou, K. S. Weil, J. Power Sources, accepted.
[19] C.-K. Lin, T.-T. Chen, Y.-P. Chyou, L.-K. Chiang, J. Power Sources 164 (2007) 238.
[20] N. Christiansen, S. Kristensen, H. Holm-Larsen, Solid Oxide Fuel Cells VIII, 2003, p. 105.
[21] J. Malzbender, R.W. Streinbrech, J. Eur. Ceram. Soc. 27 (2007) 2597.
[22] K.S. Weil, B.J. Koeppel, Int. J. Hydrogen Energy, in press, available online February 21, 2008.
[23] K.S. Weil, C.A. Coyle, J.T. Darsell, G.G. Xia, J.S. Hardy, J. Power Sources 152 (2005) 97.
[24] R.J. Svoboda, H. Simpkins, J. Keller, V.L. Sprenkle, K.D. Meinhardt, N.L. Canfield, U.S. Patent 20,050,202,159, issued 09/15/2005.
[25] J. Malzbender, T. Wakai, R.W. Steinbrech, Fuel Cells 6 (2006) 123.
[26] K.P. Recknagle, R.E. Williford, L.A. Chick, D.R. Rector, M.A. Khaleel, J. Power Sources 113 (2003) 109.
[27] S. Campanari, P. Iora, Fuel Cells 5 (2005) 34.
[28] Y. Yang, G. Wang, H. Zhang, W. Xia, J. Power Sources 167 (2007) 398.